American Mineralogist, Volume 99, pages 890–897, 2014

MINERALS IN THE HUMAN BODY

A novel technique for fluorapatite synthesis and the thermodynamic mixing behavior of F-OH apatite crystalline solutions†

GUY L. HOVIS[1,*], FRANCIS M. MCCUBBIN[2], HANNA NEKVASIL[3], GOKCE USTUNISIK[4], WILLIAM R. WOERNER[3] AND D.H. LINDSLEY[3]

[1]Department of Geology and Environmental Geosciences, Lafayette College, Easton, Pennsylvania 18042, U.S.A.
[2]Institute of Meteoritics, Department of Earth and Planetary Sciences, University of New Mexico, Albuquerque, New Mexico 87131, U.S.A.
[3]Department of Geosciences, Stony Brook University, Stony Brook, New York 11794, U.S.A.
[4]Department of Earth and Planetary Sciences, American Museum of Natural History, New York, New York 10024-5192, U.S.A.

ABSTRACT

Successful synthesis of fluorapatite has been achieved through ion-exchange between NIST hydroxlyapatite SRM 2910a and optical-grade fluorite. Additional intermediate F-OH apatite compositions were made through ion-exchange between the newly synthesized fluorapatite and the original hydroxylapatite. Based on solution calorimetric data collected on seven fluorapatite–hydroxlyapatite crystalline solutions at 50 °C in 20.0 wt% HCl under isoperibilic conditions, fluorine-rich series members display ideal thermodynamic behavior, whereas hydroxyl-rich compositions show negative enthalpies of F-OH mixing. Unit-cell volumes for the series are linear with composition. Relative to enthalpy and volume, therefore, there are no energy barriers to complete solid solution between the F and OH end-members.

Keywords: Apatite (F-OH), solution calorimetry, enthalpy, volume, thermodynamic mixing properties

INTRODUCTION

Apatite, $A_5(XO_4)_3Z$, is a common mineral in igneous and metamorphic rocks with Ca in the A site and P in the X site (Hughes and Rakovan 2002). It exhibits primary continuous solid solution through substitution of F, Cl, and OH in the Z site. It can further contain various trace elements, in the A site, making it of particular use in petrologic trace element studies and in materials design. However, the importance of the Z-site constituents, F, Cl, OH, to petrology has also been recognized (e.g., Hovis and Harlov 2010). The recent discovery that the lunar interior was not as dry as has been the long-held presumption was based in large part on OH abundance in apatite (e.g., McCubbin et al. 2010a). In spite of its obvious importance, however, the stability of the solid solution remains poorly known. A fundamental step in understanding ternary apatite stability is evaluation of the thermodynamic mixing properties.

An initial attempt at characterizing the thermodynamic mixing properties in this system addressed the thermodynamic effects of F-Cl substitution (Hovis and Harlov 2010; Schettler et al. 2011). These studies, along with structural studies (e.g., McCubbin et al. 2008), demonstrated the difficulty in both synthesizing specific apatite stoichiometries and chemical quantification of Z-site occupancy. For example, the synthesis methods employed in the work of Hovis and Harlov (2010) introduced an apparent oxyapatite chemical component into Cl-rich samples. Without knowing the quantitative effect of oxyapatite substitution on enthalpies of the samples, it was impossible to choose between two possible interpretations of the solution calorimetric data: (1) ideal thermodynamic F-Cl mixing based on non-oxyapatite-containing samples only or (2) substantial positive F-Cl enthalpies of mixing based on data for all specimens. Additional compositional uncertainty extends to all Cl-bearing samples in that there is the strong potential for OH substitution, even with efforts taken to avoid it. Other than via SIMS, which requires well-characterized apatite samples for standards, direct spot analysis for OH is not possible. For compositionally controlled synthetic apatite, it is possible to determine OH by difference in the ternary system, but this involves assuming no oxy-component and that reliable F analyses can be obtained. McCubbin et al. (2010) have discussed the F analytical problems at length.

SAMPLE SYNTHESIS

Ion-exchange between hydroxlyapatite and fluorite

The use of ion exchange (e.g., Hovis 1988; Hovis and Roux 1993, 2008) with exchange medium CaF_2, as a mechanism of converting well-characterized hydroxlyapatite into fluorapatite was explored to minimize the likelihood of incorporating significant oxycomponent in fluorapatite during synthesis. The hydroxlyapatite used was standard reference material SRM 2910a, which according to the NIST certificate of analysis is material synthesized "for use in evaluating the physical and chemical properties of calcium apatites of biological, geological, and synthetic origin." The certificate also gives an analyzed calcium content of 38.89 ± 0.85 wt%, which is 1.00 wt% less than the

* E-mail: hovisguy@lafayette.edu

† Special collection papers can be found on GSW at http://ammin.geoscienceworld.org/site/misc/specialissuelist.xhtml. Open access: Article available to all readers via GSW (http://ammin.geoscienceworld.org) and the MSA web site.

0003-004X/14/0506–890$05.00/DOI: http://dx.doi.org/10.2138/am.2014.4750

ideal 39.89 wt%, but only slightly outside the uncertainty of the NIST measurement. The phosphorous content given, 18.029 ± 0.071 wt%, is less than the ideal 18.50 wt%. However, the Ca/P molar ratio of 1.667 ± 0.037 determined from the NIST analyses equates to the ideal Ca/P ratio.

The SRM 2910a prepared by NIST utilized solution reaction of calcium hydroxide and phosphoric acid at relatively low temperatures (near the boiling point of water), as described in the certificate of analysis (synthesis procedure of McDowell et al. 1977). Interestingly, comparison of measured unit-cell dimensions of the NIST hydroxlyapatite sample as received and after annealing at 750 °C for 3 days showed clear changes beyond the standard errors of the determinations (results for SRM 2910a included in Table 3). Although such changes cannot be attributed to a particular cause, decarbonation of the original sample is one possibility. Although NIST took precautions to avoid incorporation of CO_2 into its sample, no reported measurements tested for the presence of carbonate in the sample. Dehydration of structural water, which has been observed in apatite (Yoder et al. 2012), is another possible cause of the observed change.

To have a perfectly flat surface for the ion exchange trial and to utilize chemically pure CaF_2, polished optical grade fluorite disks (e.g., 50 mm diameter × 6 mm thick) were obtained from International Crystal Laboratories (Garfield, New Jersey). A thin layer (<<1 mm) of hydroxlyapatite SRM 2910a (previously annealed at 750 °C for 72 h) fine powder was spread across the surface of a CaF_2 disk and tamped down with a spatula. The disk+powder assemblage was placed in a furnace atop a sheet of gold foil and heated in air to 750 °C. As experience with this procedure increased, three days became the typical duration of an experiment. After cooling, the assemblage was removed and the powder carefully scraped off and collected. The product then was reacted a second time under the same conditions, but using a fresh fluorite surface. Typically, the original clear fluorite surface became cloudy during the course of each synthesis reaction. Successful F-exchange in the experiments was gauged through X-ray powder diffraction analysis, which showed obvious changes in peak positions, and also unit-cell dimensions, from hydroxlyapatite to fluorapatite, as demonstrated by the data in Table 3.

Several intermediate F-OH apatite compositions were synthesized by combining carefully weighed (and dried) hydroxlyapatite and newly synthesized fluorapatite powders. Each mixture was stirred by hand with a spatula on weighing paper, then tamped down in the bottom of a small cylindrical Pt crucible and annealed at 750 °C for 72 h. These samples were remixed once each day, then tamped down again and put back into the furnace for further annealing. Although the samples were stored in a desiccator, following the first round of calorimetric experiments, the samples were reheated at 750 °C for 20.7 h in an attempt to drive off any adsorbed H_2O or CO_2 prior to the second round of calorimetric work. Synthesis conditions for each sample are summarized in Table 1.

Direct synthesis of end-member fluorapatite

The concerns with inadvertent incorporation of possible oxy- and hydroxylapatite component in fluorapatite during synthesis caused us to explore an additional method for fluorapatite synthesis using CaF_2 and β tri-calcium phosphate (TCP), both of which were purchased "off-the-shelf." To ensure proper calcium:phosphate ratios in the synthetic apatite, a representative aliquot of the batch of commercial TCP used was analyzed by X-ray diffraction. Through Rietveld analysis, it was found to contain 7 mol% calcium pyrophosphate ($Ca_2P_2O_7$). This Ca-deficiency was corrected by adding $CaCO_3$ and then decarbonating. X-ray analysis of the corrected material showed 100% TCP, and there was appropriate weight loss for 100% decarbonation.

Care was taken to avoid OH incorporation by careful drying of the starting materials. CaF_2 and corrected TCP were individually dried at 1100 °C for 1 day. Appropriate aliquots were weighed and combined in an agate mortar, mixed under alcohol for 1 h, and dried by heatlamp. The powdered mixture was added to a long Pt capsule that had been welded shut at the bottom; the top was then gently crimped closed. The Pt tube was loaded into a silica glass tube, the silica glass tube was melted above the capsule using a torch, and a capillary was pulled. The capillary and attached silica glass ampoule containing the capsule, was attached to a vacuum pump and evacuated. The powdered sample was further dried by heating at ~800 °C while still attached to the vacuum pump. The evacuated silica tube was then sealed by melting the capillary with a torch, and the ampoule was placed in a horizontal furnace at 900 °C for 23 days and then in a Deltech furnace at 1190 °C for an additional 11 days.

Sample chemistry

H_2O analysis of synthetic F-OH apatite powders by continuous flow mass spectrometry

Continuous flow mass spectrometry (CFMS) was used to quantify water contents in six of the synthetic apatites used in the

Table 1. Sample synthesis histories

Starting material	Mole fraction fluorine	*T* (°C) (±3°)	Time (h)	Product number	Further experiment on same product	*T* (°C)	Time (h)	Product number
SRM 2910a	0	755	72.1	1115				
SRM 2910a	0	755	72	1121				
SRM 2910a	0	756	72	1123				
SRM 2910a	0	753	72	1124				
SRM 2910a	0	754	72	1130	dried 1130	750	23.8	1138
1121 and 1124 hydroxylapatite + 1127 fluorapatite	0.118	754	72	1132	dried 1132	759	20.7	1143
1124 hydroxylapatite + 1117 fluorapatite	0.279	756	71.7	1128	dried 1128	759	20.7	1140
1121 hydroxylapatite + 1117 fluorapatite	0.442	755	72.2	1125	dried 1125	759	20.7	1139
1124 hydroxylapatite + 1117 fluorapatite	0.594	756	71.7	1129	dried 1129	759	20.7	1141
1123 and 1124 hydroxylapatite + 1117 fluorapatite	0.720	754	72	1131	dried 1131	759	20.7	1142
1115 hydroxylapatite + fluorite	0.85	750	41.8	1116	2nd ion exchange 1116 + fluorite	752	44.6	1117
1123 and 1124 hydroxylapatite + fluorite	0.85	756	42.3	1126	2nd ion exchange 1126 + fluorite	757	39.3	1127

TABLE 2. Electron microprobe analyses of synthetic apatite powders and one natural apatite

Oxide	1138[a] (N = 27)	1139[a] (N = 25)	1140[a] (N = 29)	1141[a] (N = 30)	1142[a] (N = 27)	1143[a] (N = 28)	NMNH 144954-3 (N = 15)
P_2O_5	42.75(51)	42.56(44)	42.72(50)	42.81(46)	42.65(36)	42.74(53)	41.67(30)
SiO_2	–	–	–	–	–	–	0.29(5)
Ce_2O_3	–	–	–	–	–	–	0.53(3)
Y_2O_3	–	–	–	–	–	–	0.06(1)
FeO	–	–	–	–	–	–	0.03(2)
MnO	–	–	–	–	–	–	b.d.
MgO	–	–	–	–	–	–	b.d.
CaO	55.46(51)	55.47(43)	55.37(64)	55.16(54)	55.25(42)	55.40(54)	54.19(24)
Na_2O	–	–	–	–	–	–	0.23(1)
SO_3	–	–	–	–	–	–	0.28(4)
H_2O[c]	1.82(5)	1.02(2)	1.30(4)	0.73(3)	0.54(1)	1.63(4)	0.09(2)
F	0.00	1.70(17)	1.06(14)	2.26(10)	2.91(21)	0.47(11)	3.46(8)
Cl	–	–	–	–	–	–	0.41(3)
–O≡F	0.00	0.72	0.45	0.95	1.23	0.20	1.45
–O≡Cl	0.00	0.00	0.00	0.00	0.00	0.00	0.09
Total	100.03	100.03	100.00	100.01	100.12	100.04	99.75
			Structural formulae based on 13 anions				
P	3.02	3.01	3.02	3.03	3.02	3.01	2.98
Si	–	–	–	–	–	–	0.02
Ce	–	–	–	–	–	–	0.02
Y	–	–	–	–	–	–	0.00
Fe	–	–	–	–	–	–	0.00
Mn	–	–	–	–	–	–	0.00
Mg	–	–	–	–	–	–	0.00
Ca	4.96	4.97	4.95	4.93	4.95	4.94	4.90
Na	–	–	–	–	–	–	0.04
S	–	–	–	–	–	–	0.02
∑ Cations	7.98	7.98	7.97	7.96	7.97	7.95	7.98
F	0.00	0.45	0.28	0.60	0.77	0.12	0.92
Cl	–	–	–	–	–	–	0.06
OH[c]	1.01	0.57	0.72	0.40	0.30	0.90	0.03
∑ Anions	1.01	1.02	1.00	1.00	1.07	1.02	1.01
OH[b]	1.00	0.55	0.72	0.40	0.23	0.88	0.02

Notes: 1σ standard deviations for each of the values are provided parenthetically. N = number of analyses per average.
[a] Analyses normalized to 100%, original sums were on average 60 ± 4 wt% due to epoxy overlap.
[b] Calculated assuming that 1 – Cl – F = OH apfu.
[c] Measured by continuous flow mass spectrometry (1138: N = 5; 1139: N = 4; 1140: N = 4; 1141: N = 3; 1142: N = 3; 1143: N = 3; NMNH 144954-3: N = 3).

present study. Measurements were made in the continuous flow mass spectrometry lab in the Department of Earth and Planetary Sciences at the University of New Mexico, using the technique and apparatuses previously described in detail by Sharp et al. (2001). Briefly, the technique involves reduction of structural OH components in solid mineral samples by reaction with glassy carbon at high temperatures. H_2 is produced by reaction of the mineral sample with carbon at 1450 °C in a helium carrier gas. Product gases are separated in a gas chromatograph and analyzed in a mass spectrometer configured to make hydrogen isotope analyses in continuous flow mode. In the present study, the sample powders were dried in a desiccated drying oven at about 100 °C and stored at these conditions until the synthetic apatite powders were wrapped in silver foil and weighed. Next, the samples were placed back into the drying oven until analysis. Each sample was weighed again before analysis to confirm the absence of either weight gain or loss. At the time of analysis, each sample was dropped into the furnace using a commercially available autosampler (e.g., Carlo Erba AS 200-LS) mounted directly over the reduction tube. Sample sizes of 3 to 9 mg provided a satisfactory amount of H_2 that was well above the detection limit and did not saturate the spectrum. McCubbin et al. (2012) demonstrated that the blank associated with sample introduction or from the silver itself was approximately 300 ppm H_2O (0.0001 μL_{H_2O}/mg powder), which was attributed to adsorbed surface water. All analyses were well above this detection limit. Throughout the analysis routine, reproducibility of the column was checked using several H_2O standards including Water Canyon biotite (USGS sample number 3149-11), BUD biotite (Bindeman and Serebryakov 2011), Banco Bonito biotite, and San Antonio biotite. For each synthetic apatite sample, we analyzed 3 to 5 separate aliquots of sample to test for homogeneity among aliquots of apatite powder. The 2σ uncertainty reported in Table 2 refers to the variability of the water contents among all of the analyses of a given sample, which was larger than the analytical uncertainty. Total time of analysis was less than two minutes for a single hydrogen analysis. Water contents for the synthetic apatite powders analyzed are presented in Table 2.

Electron probe microanalysis (EPMA) of synthetic F-OH apatite powders

Six of the synthetic apatite powders were analyzed using the JEOL 8200 electron microprobe in the Institute of Meteoritics at the University of New Mexico using Probe for EPMA (PFE) software. An accelerating voltage of 15 kV and a nominal probe current of 25 nA were used during each analysis. We conducted energy-dispersive spectroscopic measurements of the apatite powders to determine what elements needed to be included in the quantitative routine, and only peaks for Ca, P, and F were identified, indicating that possible contaminants introduced

during synthesis could not be detected. F was analyzed using a light-element LDE1 detector crystal and standardized using strontium fluoride. Ca and P were standardized using a Durango apatite standard from the UNM EPMA laboratory. A 5 μm spot was used for standardization and analysis of all apatite samples. The sample powders were so fine-grained that it was not possible to conduct individual analyses on single grains; instead, the powders were mounted in epoxy and the epoxy-impregnated powders analyzed as per the techniques discussed for powder analysis by EPMA in Reed (2005). This resulted in consistently low EPMA totals, as only Ca, P, and F were analyzed and major elements in epoxy (primarily C, O, H) ignored. To both assess the quality of the data set and obtain useable compositions, approximately 30 spots of each powder/epoxy mixture were analyzed and the average structural formula of each sample calculated. The resulting structural formula for each sample was typically within ~1% of the expected stoichiometry for P and 1.5% for Ca, giving confidence that the resulting atomic ratios were reliable.

Several authors have documented that fluorine X-ray count rates change with time as a function of crystallographic orientation during electron microprobe analysis of apatite (Stormer et al. 1993; Goldoff et al. 2012; McCubbin et al. 2010b, 2011). Given the lack of control over the orientation of the powders and likelihood of equal representation of all grain orientations, F analyses of the apatite/epoxy mixtures were monitored for time-dependent count rates; it was discovered that fluorine count rates were not always constant during the course of an analysis. For the purposes of the present study, any analysis that displayed a variable fluorine X-ray count rate was excluded. Although F is not a major constituent of the epoxy used, its presence has been confirmed by SIMS techniques (McCubbin et al. 2010b). To blank-correct for this F in the epoxy, the epoxy/F-free hydroxylapatite mixture (sample 1138) was analyzed for F and found to contain 0.07 ± 0.03 wt% F. This value was used to blank-correct all of the other analyses. A summary of all EPMA analyses is provided in Table 2.

Hydroxyl cannot be measured directly by the EPMA technique; however, a missing structural component in the anion site of the apatite can be calculated on the basis of stoichiometry to compare with the CFMS results. If the other anions in the site are analyzed with sufficient accuracy (in our case F^-), this missing component can be attributed to some combination of the anions Cl^-, OH^-, O^{2-}, CO_3^{2-}, S^{2-}, Br^-, and I^- and/or structural vacancies (Pan and Fleet 2002) and/or structural H_2O (Yoder et al. 2012; Mason et al. 2009). The most likely culprit for this missing component in our synthetic system is OH^- or structural vacancies, due to compositional limitations imposed by the synthesis technique utilized.

Chemistry of additional synthetic and natural specimens

The most F-rich sample obtained by ion-exchange between fluorite and hydroxlyapatite could not be analyzed by the techniques above due to both the fine-grain size of the sample, and because of anticipated low levels of OH that were thought to be well below the detection limit for H_2O by continuous flow mass spectrometry. To determine the composition of F-rich samples 1117 and 1127, anticipated compositions of intermediate F-OH members (based on sample weights and an assumed pure fluorapatite end-member) were plotted against the actual (measured) compositions determined by the techniques above. The resulting well-defined linear trend was utilized to yield an F:OH ratio of 0.85:0.15 for samples 1117 and 1127 (which have identical unit-cell dimensions within a single standard deviation). On subsequent plots of unit-cell dimension data it is seen that this composition fits well with data for other samples, which supports the determined composition. Although no pure-F end-member was synthesized by the F-OH ion-exchange experiments, data for the fluorapatite end-member were obtained using the samples synthesized at high temperatures (SB fluorapatite 4-13-11, described above, and fluorapatite APS-25 from Hovis and Harlov 2010).

A natural apatite specimen was obtained from the National Museum of Natural History to compare data for the newly synthesized samples with those for a naturally occurring apatite sample. The chemical analysis for Durango (Mexico) fluorapatite NMNH 144954-3 is included in Table 2 (compare with Young et al. 1969). Of course, natural samples present problems of their own, including the propensity for cationic and anionic substitutions that remove them from the simple F-OH binary system, as well as the possibility for chemical heterogeneity.

Characterization by X-ray powder diffraction

The unit-cell dimensions of all F-OH apatite samples were determined using data acquired with a Scintag PAD V X-ray powder diffractometer. Scans using Cu radiation typically were run from 15 to 72° 2Θ at a rate of 0.25°/min. NIST SRM 640a silicon, with a stated unit-cell dimension of 5.430825 Å, was used as an internal standard. Indexing of hydroxlyapatite X-ray diffraction maxima was aided by XRD data given in the NIST certificate of analysis. There also are additional sources of XRD data for fluorapatite and hydroxylapatite, such as the ICDD database. Additionally, peaks were tracked from the OH to the F end of the ion-exchange series, and vice versa; this was especially helpful for mid-compositions for which XRD data are sparse or nonexistent. Calculations of unit-cell dimensions were made using the unit-cell program of Holland and Redfern (1997).

It should be noted that X-ray diffraction maxima for the original SRM-2910a were not as sharp as those of typical well-crystallized mineral samples. Almost certainly this is related to the relatively low-temperature and rapid synthesis conditions utilized by NIST, which likely produced a sample that was less crystalline than natural geological samples. Nevertheless, XRD data for the specimens synthesized by ion exchange show well-defined peaks having 2Θ positions that are easily measured.

Solution calorimetry

The calorimetric system used to measure enthalpies of solution has been described in Hovis and Roux (1993) and Hovis et al. (1998). The latter paper demonstrates that this system enables the measurement of precise enthalpies of solution for samples as small as 10 mg. In the present study apatite sample weights ranged from 48.7 to 52.2 mg.

Because of the production of CaF_2 as a precipitate (fluorite) or gel, it is not possible to conduct dissolutions of F-bearing apatite in the standard solvent (20.1 wt% hydrofluoric acid) employed by the Lafayette College solution calorimetry laboratory (see more

extensive discussion in Hovis and Harlov 2010). For the present study, therefore, each apatite dissolution was performed in 20.0 wt% hydrochloric acid (910.1 g, or ~1 L). All experiments took place at 50 °C under isoperibolic conditions (i.e., temperature of the water bath surrounding the calorimeter held constant) utilizing an internal sample container (Waldbaum and Robie 1970). In all cases, only one dissolution was performed in each liter of acid so as to minimize the amount of fluorine in solution.

Dissolutions for the calorimetric experiments on the ion-exchanged samples were performed on powders having the relatively fine grain sizes inherited from the original SRM 2910a hydroxylapatite. It is known that heat effects can arise from extremely fine grains (Nitkiewicz et al. 1983). If these arose, they would have occurred for all ion-exchange series samples, as all such samples had essentially the same grain sizes; this suggests that compositional differences should be robust. The additional deleterious effect of fine grains comes during weighing of samples for calorimetry as they tend to be hygroscopic. Adsorbed water can cause additional weighing uncertainties, which in turn, affect both calorimetric accuracy and precision. On the other hand, fine grains also can increase calorimetric precision by promoting rapid dissolution, resulting in less heat exchange between the calorimeter and its environment, and in turn a smaller ΔT correction for the sample dissolution period. Overall, however, calorimetric precision for the present samples is somewhat less than that experienced in previous work on silicate mineral systems, probably due to the H_2O-weight-gain issue. Importantly, grain-size effects would not have been an issue either for the relatively coarse high-temperature synthetic fluorapatite sample SB fluoraparite 4-13-11 nor for the two natural apatite samples. The fact that data for these samples are compatible with those from samples of the ion-exchange series suggests that small grain size was not a major source of calorimetric uncertainty.

Resulting data

Unit-cell dimensions and volumes

The unit-cell dimensions and volumes calculated from X-ray powder diffraction data are given in Table 3 and plotted in Figures 1 to 3. Figure 1 demonstrates the linear behavior of the *a* unit-cell dimension with composition. Extension of the fitted line intersects the data point for fluorapatite SB 4-13-11 and comes within a few tenths of an angstrom of intersecting the APS-25 fluorapatite data point of Hovis and Harlov (2010).

The *c* unit-cell dimension (Fig. 2) changes little, if at all, with composition, as all *c* values are within 0.01 Å of one another. The projected data point at $X_F = 1.0$ in Figure 2 fits well with the datum for APS-25 (ibid). On the other hand, the *c*-value for fluorapatite SB 4-13-11 falls somewhat below the others. The reason for this is unknown, but in all likelihood represents slight differences in chemical composition (e.g., hydroxyl or oxy component abundances) between the pure fluorapatite samples.

The unit-cell volume (Fig. 3) behaves linearly with composition. It can be described by

$$V\ (\text{Å}^3/\text{unit cell}) = 528.78 - 5.664\ X_F \quad (1)$$

and fits well with data for APS-25 (ibid). The lower volume for fluorapatite SB 4-13-11 is related to the lower value for *c*. Linear behavior of volume with regard to composition was seen as well for F-Cl apatite crystalline solutions (Schettler et al. 2011; Hovis et al. 2011). This linearity is important for the thermodynamic implications discussed below.

Table 3. Unit-cell data for F-OH apatite samples

Sample	Mole fraction F	*a* (Å)	c (Å)	Volume (Å³)
SRM 2910a	0	9.4214(10)	6.8891(11)	529.58(12)
1121	0	9.4167(6)	6.8853(7)	528.75(7)
1123	0	9.4171(4)	6.8831(5)	528.62(5)
1124	0	9.4177(6)	6.8845(8)	528.81(7)
1130	0	9.4177(5)	6.8841(7)	528.77(6)
1132	0.118	9.4120(5)	6.8826(7)	528.02(6)
1128	0.279	9.4054(4)	6.8851(5)	527.47(5)
1125	0.442	9.3954(5)	6.8860(8)	526.42(6)
1129	0.594	9.3867(5)	6.8870(7)	525.52(6)
1131	0.720	9.3795(4)	6.8852(4)	524.57(4)
1117	0.85	9.3732(5)	6.8862(6)	523.94(6)
1127	0.85	9.3734(6)	6.8853(8)	523.90(7)
Fluorapatite SB 4-13-11[a]	1.0	9.3660(3)	6.8765(6)	522.40(5)
Fluorapatite SB 4-13-11[b]	1.0	9.366815(37)	6.876535(36)	
Fluorapatite APS-25[c]	0.999	9.3697(4)	6.8849(4)	523.46(4)
Fluorapatite APS-25[a]	0.999	9.3697(2)	6.8847(6)	523.44(3)

Note: One standard deviation in final decimal place(s) given in parentheses.
[a] Determined at Lafayette College on a Scintag Pad V X-ray diffraction unit using NIST 640a Si internal standard.
[b] Determined at Stony Brook University on a Rigaku Ultima IV X-ray diffraction unit using a zero-background quartz sample holder.
[c] From Schettler et al. (2011).

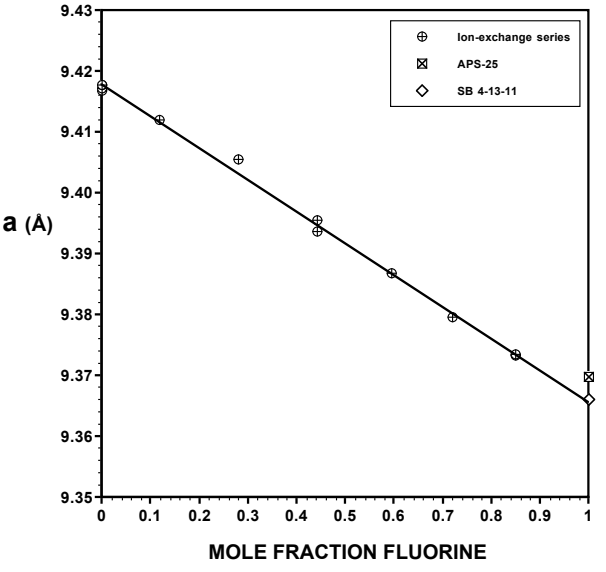

Figure 1. The *a* unit-cell dimension plotted against mole fraction fluorine in the Z site (X_F) for the F-OH apatite ion-exchange series, as well as high-temperature synthetic fluorapatite samples SB 4-13-11 (this study) and APS-25 (Hovis and Harlov 2010). The size of the data points (~0.002 Å high) may be compared with the standard deviations for *a* values in Table 3. The fitted line, $R^2 = 0.998$, *a* (Å) = 9.4177–5.2184 X_F, is based only on ion-exchanged samples (circles), not fluorapatite end-members.

Enthalpies of solution and F-OH mixing

Solution calorimetric data for the newly synthesized F-OH apatites are given in Table 4. As noted in previous papers, it is advantageous to plot negative values for these data; this allows concave-down relationships to be associated with positive heats

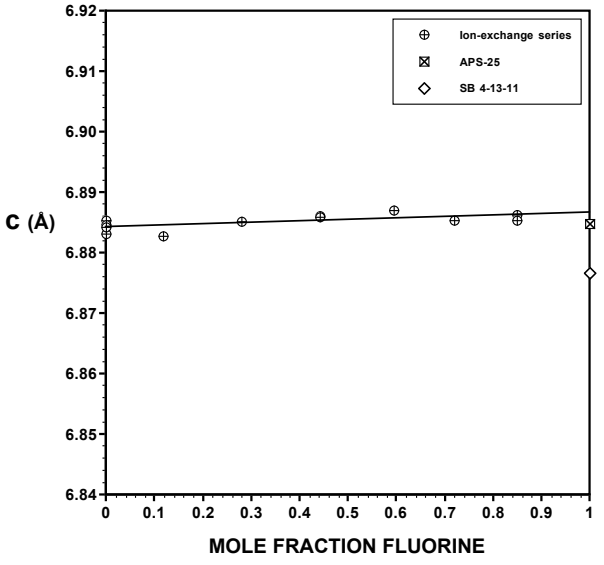

FIGURE 2. The *c* unit-cell dimension plotted against mole fraction fluorine in the Z site (X_F) for F-OH apatite crystalline solutions. The size of the data points (~0.002 Å high) may be compared with the standard deviations for *c* values in Table 3. The fitted line, $R^2 = 0.443$, *c* (Å) = 6.8841 + 0.0024 X_F is based only on ion-exchanged samples (circles), not fluorapatite end-members.

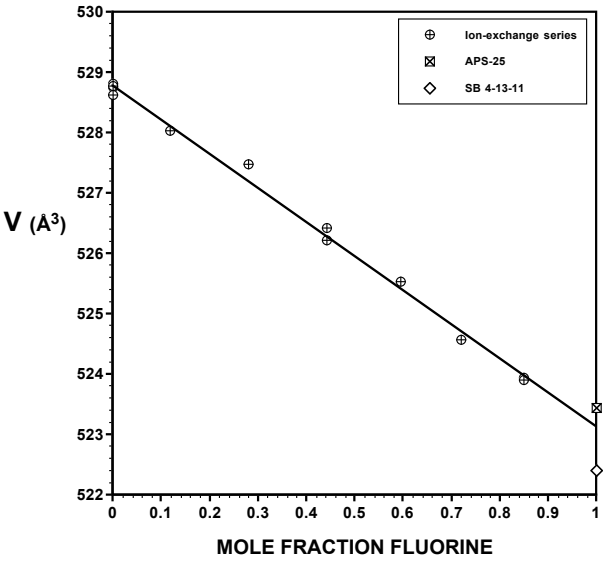

FIGURE 3. Unit-cell volume plotted against mole fraction fluorine in the Z site (X_F) for F-OH apatite crystalline solutions. The size of the data points (~0.18 $Å^3$ high) may be compared with the standard deviations for volumes in Table 3. The fitted line, $R^2 = 0.996$, *V* ($Å^3$) = 528.78 – 5.664 X_F, is based only on ion-exchanged samples (circles), not fluorapatite end-members.

of mixing and concave-up curves to be related to negative ones. Accordingly, negative values for heats of solution are plotted against mole fraction fluorine in the Z-site (Fig. 4). A third-order polynomial fits the data well.

$$-H_{soln}\ (kJ/mol) = 143.95 - 134.72\ X_F + 121.38\ X_F^2 - 82.654\ X_F^3 \quad (2)$$

The magnitude of excess enthalpy, which relates to the energetics of non-ideal mixing of the fluor- and hydroxlyapatite components, depends upon the ideal mixing line chosen. Under optimal conditions, this is determined from the enthalpy of solution of the end-members in identical structural states. The differences in enthalpy of solution of the fluorapatite samples and the extrapolated ion-exchanged fluorapatite composition, makes the choice of an ideal mixing line more difficult. On the other hand, it is reasonable to consider the calorimetric results for the F-OH ion-exchange series independently of other data due to the "connectedness" of the samples via the synthesis methods used to make them. With that in mind, a line can be drawn from the hydroxlyapatite end-member through the most F-rich member of the F-OH series at $X_F = 0.85$. Such a line is described by the equation

$$-H_{soln}\ (kJ/mol) = 143.95 - 90.41\ X_F. \quad (3)$$

Coincidentally, this line passes through data for the F-rich sample at $X_F = 0.720$ and comes close as well to the data at $X_F = 0.594$. Extension of the line to $X_F = 1.0$ nearly intersects fluorapatite end-member data for both SB 4-13-11 and Durango NMNH 144954-3 after data for the latter have been corrected for Cl content (6.77 kJ/mol), based on the ideal enthalpy model

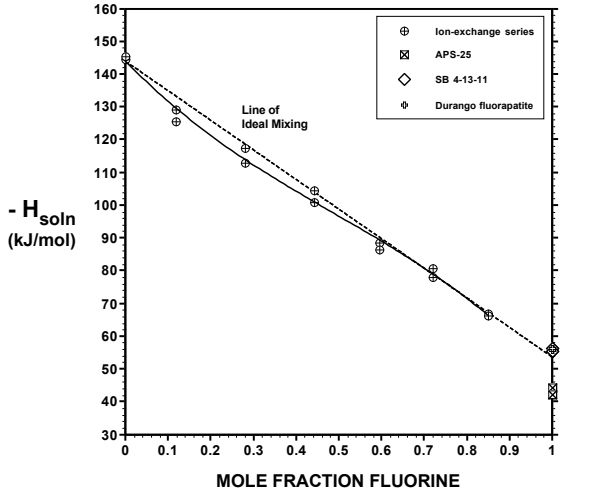

FIGURE 4. Negative enthalpies of solution plotted against mole fraction fluorine in the Z site (X_F) for F-OH apatite crystalline solutions (circles). Each symbol represents the data for one solution calorimetric experiment, although each experiment yields two (similar, so superimposed) data points based on calorimeter heat capacities measured before and after dissolution (see Table 4). The solid curve fitted to the calorimetric data correlates with Equation 2. Development of the dashed line for ideal mixing, Equation 3, is discussed in the text. Squares are data for sample APS-25 of Hovis and Harlov (2010). The two (nearly coincident) data points at $X_F = 1$ are for synthetic fluroapatite SB 4-13-11 (open diamonds) and natural Durango fluorapatite NMNH 144954-3 (small crosses inside the open diamonds), the latter having been corrected for chlorine content based on the ideal F-Cl apatite mixing model of Hovis and Harlov (2010). Precision of the calorimetric data is reflected by reproducibility, as evidenced by duplicate experiments at each composition.

TABLE 4. Solution calorimetric data

Sample number	Sample name	Mole fraction F	Gram formula weight (g/mol)	Sample weight (g)	Temperature change during dissolution (°C)	Mean solution temperature (°C)	Calorimeter heat capacities before and after dissolution (J/°)		Enthalpies of solution based on the two heat capacities (kJ/mol)	
							I	II	I	II
Synthetic (mostly ion-exchanged) F-OH apatite samples from Lafayette College (as described in the text)										
1121	hydroxylapatite	0.000	502.3114	0.05104	0.004450	49.944	3303.6	3303.0	−144.40	−144.37
1138	hydroxylapatite	0.000	502.3114	0.05037	0.004432	49.985	3299.5	3299.7	−145.54	−145.69
1132	apatite (F-OH ss)	0.118	502.5463	0.05002	0.003883	49.971	3302.6	3302.7	−129.08	−129.09
1143	apatite (F-OH ss)	0.118	502.5463	0.05002	0.003790	49.983	3304.1	3304.2	−125.58	−125.57
1128	apatite (F-OH ss)	0.279	502.8669	0.05010	0.003545	49.969	3303.8	3303.6	−117.31	−117.31
1140	apatite (F-OH ss)	0.279	502.8669	0.05014	0.003409	49.973	3305.0	3305.1	−112.76	−112.76
1125	apatite (F-OH ss)	0.442	503.1915	0.05019	0.003161	49.997	3303.7	3303.1	−104.48	−104.45
1125	apatite (F-OH ss)	0.442	503.1915	0.05008	0.003044	49.972	3304.2	3303.3	−100.85	−100.82
1129	apatite (F-OH ss)	0.594	503.4941	0.05017	0.002677	49.975	3303.9	3303.2	−88.60	−88.58
1141	apatite (F-OH ss)	0.594	503.4941	0.05011	0.002607	49.979	3304.6	3304.7	−86.40	−86.40
1131	apatite (F-OH ss)	0.720	503.7450	0.04874	0.002365	49.975	3304.3	3303.6	−80.59	−80.58
1142	apatite (F-OH ss)	0.720	503.7450	0.05033	0.002363	49.978	3304.8	3304.9	−78.01	−78.03
1117	fluorapatite by ion exchange	0.850	504.0038	0.05001	0.002010	49.974	3303.3	3300.1	−66.79	−66.72
1127	fluorapatite by ion exchange	0.850	504.0038	0.04918	0.001965	50.028	3304.1	3303.4	−66.41	−66.40
Synthetic fluorapatite from Stony Brook University (as described in the text)										
SB 4-13-11	fluorapatite	1.0	504.3025	0.04923	0.001667	49.977	3312.6	3312.7	−56.44	−56.44
SB 4-13-11	fluorapatite	1.0	504.3025	0.04991	0.001664	49.973	3309.0	3309.1	−55.52	−55.52
Synthetic fluorapatite of Harlov (Hovis and Harlov 2010)										
APS-25	fluorapatite	0.999	504.3253	0.05219	0.001396	49.973	3294.7	3293.6	−44.38	−44.36
APS-25	fluorapatite	0.999	504.3253	0.04901	0.001244	49.962	3295.4	3294.6	−42.14	−42.12
Natural fluorapatite from the U.S. National Museum of Natural History										
NMNH 144954-3	Durango fluorapatite	see Table 2	505.5859	0.04997	0.001869	49.973	3310.7	3310.8	−62.47	−62.45
NMNH 144954-3	Durango fluorapatite	see Table 2	505.5859	0.05012	0.002105	49.977	3309.2	3309.3	−70.13	−70.10
NMNH 144954-3	Durango fluorapatite	see Table 2	505.5859	0.05031	0.001903	49.976	3309.5	3309.6	−63.16	−63.19

of Hovis and Harlov (2010, see their Fig. 2) for the F-Cl apatite system. If the choice of end-member enthalpies of solution and hence, this ideal mixing line, is reasonable, F-rich members of the series would be interpreted as behaving ideally in a thermodynamic sense, while OH-rich samples would exhibit negative enthalpies of mixing, reflected by the concave-up fitted curve for OH-rich samples in Figure 4. The excess enthalpies of mixing (that is, those not accounted for by ideal mixing) may be expressed as

$$H_{ex}\ (kJ/mol) = 44.31\ X_F + 121.38\ X_F^2 - 82.654\ X_F \qquad (4)$$

for compositions between $X_F = 0$ and 0.679 (where $H_{ex} = 0$ for $X_F > 0.679$), and reach a maximum magnitude of –4.8 kJ/mol at $X_F = 0.24$ (Fig. 5). Although the magnitude of this excess enthalpy of mixing depends upon the choice of ideal mixing line, and therefore on the enthalpies of solution of the end-member apatites, the use of samples with similar mode of origin maximizes the likelihood that this is a reflection of true mixing characteristics.

There is a difference of ~12 kJ/mol among the three pure-fluorapatite data points (i.e., the extrapolated F-end-member of the ion-exchanged F-OH apatite series, SB 4-13-11, and APS-25). This probably represents real differences among the samples, but it is not obvious what these might be. Possibilities include differences in crystallinity (particularly for the F-OH ion exchange series), non-stoichiometry in the samples, or sample impurities of various kinds that can occur in both synthetic and natural samples. It is clear from the unit-cell dimensions that, while the properties of "pure" fluorapatite specimens from the present study may be similar, they are not identical. While choice of SB 4-13-11 as the fluorapatite end-member would only marginally increase the negative excess mixing magnitudes, use of APS-25 as the pure-F end-member would produce nearly ideal behavior for OH-rich specimens and positive excess enthalpies in the F-rich part of the series.

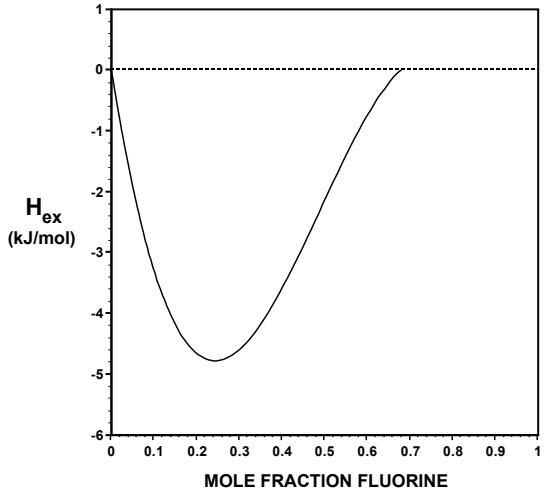

FIGURE 5. Enthalpies of mixing plotted against mole fraction fluorine for F-OH apatite crystalline solutions based on differences between the enthalpies of solution described by Equation 2 (Fig. 4) and the ideal mixing line (Eq. 3, Fig. 4), whose development is described in the text. Relationships are expressed by Equation 4.

IMPLICATIONS

The thermodynamic requirements for immiscibility within a solid-solution series is that positive excess Gibbs free energies (G_{ex}) of sufficient magnitude exist across the F-OH apatite join under some set of pressure-temperature conditions. G_{ex}, in turn

is a function of excess enthalpy (H_{ex}), volume (V_{ex}), and entropy (S_{ex}) related to F-OH mixing, where $G_{ex} = H_{ex} + PV_{ex} - TS_{ex}$ (T = absolute temperature, P = pressure). Immiscibility in turn is associated with positive values for H_{ex} and V_{ex}, but negative ones for S_{ex}.

The observed unit-cell volumes for the F-OH apatite system behave linearly with F:OH ratio, so V_{ex} is zero across the entire series. The only enthalpies of F-OH mixing in the system, based on analysis of the solution calorimetric data presented here, are negative. Barring negative entropies of F-OH mixing for this system, there is no thermodynamic barrier to complete dissolution of hydroxyl ions in fluorapatite, nor fluorine ions in hydroxylapatite, at any temperature or pressure.

If apatite is to be utilized as a petrogenetic indicator, it is essential that this chemically complex system be characterized thermodynamically. The present study of F-OH apatite solid solutions makes an essential contribution to such characterization, adding to previous data for the F-Cl apatite binary (Hovis and Harlov 2010). We hope to be able to make future contributions to additional apatite binaries (e.g., Cl-OH), as well as more complex apatite systems, as new sample synthesis methods are developed. We hope as well that the solid-solid ion-exchange synthesis techniques used to make F-OH apatites for this study, and also the techniques utilized to produce end-member synthetic fluorapatites, might encourage others to develop new synthesis methods to make possible the study of additional apatite compositions.

Acknowledgments

G.L.H. and H.N. thank the Earth Sciences Division of the US National Science Foundation for support of this research through grants EAR-1019809 and EAR-809283, respectively. F.M.M. acknowledges support for this research from the NASA Cosmochemistry Program through grant NNX11AG76G. We thank Jeffrey Post and Michael Wise of the National Museum of Natural History and George Harlow of the American Museum of Natural History for providing natural samples for this and other apatite work.

References cited

Bindeman, I.N., and Serebryakov, N.S. (2011) Geology, Petrology and O and H isotope geochemistry of remarkably ^{18}O depleted Paleoproterozoic rocks of the Belomorian Belt, Karelia, Russia, attributed to global glaciation 2.4 Ga. Earth and Planetary Science Letters, 306, 163–174.

Goldoff, B., Webster, J.D., and Harlov, D.E. (2012) Characterization of fluor-chlorapatites by electron probe microanalysis with a focus on time-dependent intensity variation of halogens. American Mineralogist, 97, 1103–1115.

Holland, T.J.B., and Redfern, S.A.T. (1997) Unit-cell refinement: Changing the dependent variable, and use of regression diagnostics. Mineralogical Magazine, 61, 65–77.

Hovis, G.L. (1988) Enthalpies and volumes related to K-Na mixing and Al-Si order/disorder in alkali feldspars. Journal of Petrology, 29, 731–763.

Hovis, G.L., and Harlov, D.E. (2010) Solution calorimetric investigation of fluor-chlorapatite crystalline solutions. American Mineralogist, 95, 946–952.

Hovis, G.L., and Roux, J. (1993) Thermodynamic mixing properties of nepheline-kalsilite crystalline solutions. American Journal of Science, 293, 1108–1127.

——— (2008) Thermodynamic mixing properties of Rb-K feldspars. American Mineralogist, 93, 1597–1602.

Hovis, G.L., Roux, J., and Richet, P. (1998) A new era in hydrofluoric acid solution calorimetry: Reduction of required sample size below ten milligrams. American Mineralogist, 83, 931–934.

Hovis, G., Harlov, D., Gottschalk, M., and Schettler, G. (2011) Unit-cell data and XRD compositional indicators for fluorapatite-chlorapatite crystalline solutions. Geophysical Research Abstracts 13, Abstract EGU2011-12014.

Hughes, J.M., and Rakovan, J. (2002) The crystal structure of apatite. In M.J. Kohn, J. Rakovan, and J.M. Hughes, Eds., Phosphates: Geochemical, Geobiological, and Materials Importance, vol. 48, p. 1–12. Reviews in Mineralogy and Geochemistry, Mineralogical Society of America, Chantilly, Virginia.

Mason, H.E., McCubbin, F.M., Smirnov, A., and Phillips, B.L. (2009) Solid-state NMR and IR spectroscopic investigation of the role of structural water and F in carbonate-rich fluorapatite. American Mineralogist, 94, 507–516.

McCubbin, F.M., Mason, H., Park, H., Phillips, B.L., Parise, J.B., Nekvasil, H., and Lindsley, D.H. (2008) Synthesis and characterization of low-OH-fluor-chlorapatite: A single crystal XRD and NMR spectroscopic study. American Mineralogist, 93, 210–216.

McCubbin, F.M., Steele, A., Hauri, E.H., Nekvasil, H., Yamashita, S., and Hemley, R.J. (2010a) Insights into hydrous magmatism on the Moon from the mineral apatite. Proceedings of the National Academy of Sciences, 107, 11223–11228, www.pnas.org/cgi/doi/10.1073/pnas.1006677107.

McCubbin, F.M., Steele, A., Nekvasil, H., Schnieders, A., Rose, T., Fries, M., Carpenter, P.K., and Jolliff, B.L. (2010b) Detection of structurally bound hydroxyl in fluorapatite from Apollo mare basalt 15058,128 using TOF-SIMS. American Mineralogist, 95, 1141–1150.

McCubbin, F.M., Jolliff, B.L., Nekvasil, H., Carpenter, P.K., Zeigler, R.A., Steele, A., Elardo, S.M., and Lindsley, D.H. (2011) Fluorine and chlorine abundances in lunar apatite: Implications for heterogeneous distributions of magmatic volatiles in the lunar interior. Geochimica et Cosmochimica Acta, 75, 5073–5093.

McCubbin, F.M., Hauri, E.H., Elardo, S.M., Vander Kaaden, K.E., Wang, J., and Shearer, C.K. (2012) Hydrous melting of the martian mantle produced both depleted and enriched shergottites. Geology, 40, 683–686.

McDowell, H., Gregory, T.M., and Brown, W.E. (1977) Solubility of $Ca_5(PO_4)_3OH$ in the system $Ca(OH)_2$-H_3PO_4-H_2O at 5, 15, 25 and 37 °C. Journal of Research of the National Bureau of Standards, 81A, 273–281.

Nitkiewicz, A.M., Kerrick, D., and Hemingway, B.S. (1983) The effect of particle size on the enthalpy of solution of quartz. Abstracts with Programs Geological Society of America, 15, 653.

Pan, Y.M., and Fleet, M.E. (2002) Compositions of the apatite-group minerals: Substitution mechanisms and controlling factors. In M.L. Kohn, J. Rakovan and J.M. Hughes, Eds., Phosphates: Geochemical, Geobiological, and Materials Importance, 48, 13–49. Reviews in Mineralogy and Geochemistry, Mineralogical Society of America, Chantilly, Virginia.

Reed, S.J.B. (2005) Electron Microprobe Analysis and Scanning Electron Microscopy in Geology, 192 p. Cambridge University Press, U.K.

Schettler, G., Gottschalk, M., and Harlov, D.E. (2011) A new semi-micro wet chemical method for apatite analysis and its application to the crystal chemistry of fluorapatite-chlorapatite solid solutions. American Mineralogist, 96, 138–152.

Sharp, Z.D., Atudorei, V., and Durakiewicz, T. (2001) A rapid method for determination of hydrogen and oxygen isotope ratios from water and hydrous minerals. Chemical Geology, 178, 197–210.

Stormer, J.C., Pierson, M.L., and Tacker, R.C. (1993) Variation of F-X-ray and Cl-X-ray intensity due to anisotropic diffusion in apatite during electron-microprobe analysis. American Mineralogist, 78, 641–648.

Waldbaum, D.R., and Robie, R.A. (1970) An internal sample container for hydrofluoric acid solution calorimetry. Journal of Geology, 78, 736–741.

Yoder, C.H., Pasteris, J.D., Worcester, K.N., and Schermerhorn, D.V. (2012) Structural water in carbonated hydroxylapatite and fluorapatite: Confirmation by solid state ^2H NMR. Calcified Tissue International, 90, 60–67.

Young, E.J, Myers, A.T., Munson, E.L., and Conklin, N.M. (1969) Mineralogy and geochemistry of fluorapatite from Cerro de Mercado, Durango, Mexico. U.S. Geological Survey Professional Paper 650-D, D84–D93.

Manuscript received September 19, 2013
Manuscript accepted January 17, 2014
Manuscript handled by Simon Redfern